Oral Presentation

The 7th TSME International Conference on Mechanical Engineering
13-16 December 2016

TSME ICOME 2016
Mechanical Engineering Innovation for Green Society

AEC0016

A modified analytical model for understanding the behaviour of slag flow inside the entrained flow gasifier

Thananan Chanchanayothin[1], Chatchawan Chichana[1], Alexander Y. Ilyushechkin [2], and San Shwe Hla[2,*]

[1] Department of Mechanical Engineering, Faculty of Engineering, Chiang Mai University, 239 Huay Kaew Rd., Muang District, Chiang Mai, THAILAND 50200
[2] CSIRO Energy, PO Box 883, Pullenvale, QLD 4069, AUSTRALIA

[*] Corresponding Author: San.Hla@csiro.au, Phone: +61 7 3327 4125, Fax: +61 7 3327 4455

Abstract

High temperature entrained flow gasification is a widely-used technology for the production of chemicals and fertilizers, and has been shown to generate electricity with reduced CO_2 emissions compared with traditional technologies using Integrated Gasification Combined Cycle (IGCC). The understanding of the behavior of slag flow along the inner wall of entrained-flow gasifier is the most critical decision-making factor for successful operation. The behaviour of slag flow inside the gasifier can be predicted numerically by solving momentum, mass and energy balance equations simultaneously with temperature-dependent slag viscosity information. However, as gasifier models are usually solved using complex numerical methods, it is often impractical and time consuming to solve another set of numerical equations within a numerical model. Therefore, several analytical models for slag flow have been previously proposed.

In this study, previously-developed slag flow models were reviewed and combined in order to apply advantages from those models as well as to reduce the impact of their limitations. Simulations were conducted applying the geometry of a $5MW_{th}$ pilot-scale gasifier under realistic operating conditions and also using temperature dependent thermophysical and transport properties for gases and slags from two Australian coals. The model can estimate both solid and liquid slag layer thickness along the wall of the gasifier and is able to calculate the radial profile of temperatures and velocities of liquid slag. More importantly, it can predict the surface temperatures of liquid slag which is essential information required for gasifier model to calculate the heat losses from gases and solids to reactor walls. The simulation results showed that this analytical model can predict the slag behaviour closely to those predicted by a numerical method under several operating conditions regardless of whether the local gas temperature is greater or smaller than the critical viscosity temperature (T_{cv}) of slags.

Keywords: Entrained-flow gasification; Slag-flow model; Analytical method; Critical viscosity temperature;

1. Introduction

High temperature entrained-flow gasification is regarded as a less carbon-intensive electricity generation option for near future. Currently, it has being successfully and commonly used to produce chemicals and fertilizers from coals. Understanding of slag behaviour under high temperature gasification condition is critical for successful and sustainable for continuous operation. During the high temperature gasification process, mineral matter in coal turn to slag and most of them deposits on the gasifier wall. Due to relatively lower temperature of gasifier wall, the slags initially solidify and the newer deposits maintain their liquid state. Sufficient amount of solid deposits essential as they act like thermal barrier in order to protect the gasifier wall from heat losses and refractory corrosion. However, if the slag layer becoming too thick, it would become an obstruction for slag tapping and lead to gasifier shut down. To achieve steady slags flow down mostly driven by gravity and discharge continuously from tap hole at the bottom of the gasifier, it is generally considered that viscosity should be within the range of 5 to 25 Pa.s at operating temperatures of 1200-1500°C [1].

As understanding of behaviour of slag flow is critically important, several researchers have modelled (both analytically and numerically) to analyze on the characteristic of the slag flow inside the entrained flow gasifiers [2-12]. While numerical models can estimated the slag flow behaviour more precisely, they are time-consuming and complicated to integrate with comprehensive gasifier models which are to be solved by complex numerical methods. By assuming or simplifying the temperature profile of the liquid slags, slag flows inside the entrained flow gasifier can be solved analytically which is simply allowed to integrate even for a complex CFD based gasifier model [2]. Among the analytical models developed for slag flow, the one that proposed by Seggiani [3] was adapted by

many researchers to apply in their reactor models. Seggiani's model assumed that temperature profile across the layer of liquid slag is linear and, viscosities were estimated as exponential function of temperatures [3]. The limitation of slag temperatures' profile being linear was modified by Yong et al. [4] who developed a modified analytical model by using a cubic temperature profile. While their assumption is more likely to represent the realistic slag temperature profiles, values of slag properties (especially viscosities) are fixed at the average temperature [4]. Although these two approaches are predominant among the analytical slag flow models, both methods have advantages and drawbacks. Ye and Ryu [12] made an assessment on performance of these two models using simulated results using their numerical model which was developed including full heat transfer processes on energy balance governing equation without any simplified assumptions. In their conclusion, Ye and Ryu [12] remarked that estimation using Seggiani's model agreed well their numerical model's prediction for all cases except when the gas temperature fell below the slag critical viscosity temperature. Unlike Seggiani' model, methods proposed by Yong et al [4] was found to be working well under that particular operating condition.

In this paper, a new analytical approach was proposed by applying advantages from both analytical methods but eliminating the impact of their limitation. Then, our analytical model was simulated using the realistic operating condition in 5MW pilot-scale gasifier and compared the simulation results with performances of existing models- namely analytical models developed by Seggiani [3] and Yong et al. [4].

2. Slag model

Slag layers in gasifier consist from so-called 'frozen' slag and flowing slag layer, which is mainly in liquid phase. For simplicity in this study we consider:

- Liquid slag has dominant liquid phase (if it has some solids, they do not distract Newtonian flow and do not increase viscosity drastically). Therefore, flow of liquid slag is assumed to be Newtonian [3,4]
- Solid slags consists from fully solid 'frozen layer' and from the slag which has dominant solid phases and non-Newtonian flow behavior.
- The transition temperature from liquid to solid stage of slag is taken the temperature of critical viscosity (T_{cv}) [3,4]
- Direction of slag flow is downward only (i.e. no reverse flow and no slag dripping) [3,4]
- Heat transfer is normal to the surface [3,4]
- The slag thickness is far too small compared to the reactor diameter [3,4]

Regarding with temperature profiles and estimation of viscosities, the following specific assumption were made in this study:

- The temperature profile across the liquid slag is assumed as cubic [4] as equation (1):

$$\square(\square,\square) = \square + \square\square + \square\square^2 + \square\square^3 \qquad (1)$$

With boundary condition:

$$\square = 0\,; \quad \square = \square_\square\,; \quad \frac{\square\square}{\square\square} = -\frac{\dot{\square}_{\square\square}}{\square}$$

$$\square = \square_\square\,; \quad \square = \square_{\square\square}\,; \quad \frac{\square^2\square}{\square\square^2} = 0$$

where $\square_\square$ is surface temperature, $\square_{\square\square}$ is critical viscosity temperature, $\dot{\square}_{\square\square}$ is heat flux from gas to slag, $\square_\square$ is liquid slag thickness, and *k* is thermal conductivity of slag.

The solution of Eq. (1) become the temperature profile across the liquid slag is given by [4]:

$$\square(\square) = \square_{\square\square} + \left\{\left[1.5(\square_\square - \square_{\square\square}) - \frac{\dot{\square}_{\square\square}\square_\square}{2\square}\right]\left(1 - \frac{\square}{\square_\square}\right)\right\} - \left\{\left[0.5(\square_\square - \square_{\square\square}) - \frac{\dot{\square}_{\square\square}\square_\square}{2\square}\right]\left(1 - \frac{\square}{\square_\square}\right)^3\right\} \qquad (2)$$

- Unlike the methods used by Yong et al. [4], temperature-dependent viscosities of the liquid slag was calculated using an approximate exponential function [3].

The key input-output parameters used in this slag flow model and the way they integrate with gasifier model are illustrated in Figure 1.

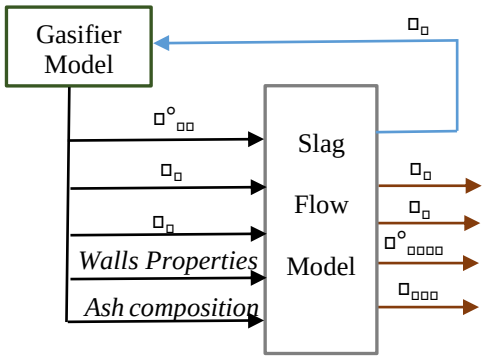

Figure 1. The scheme of input-output variables of slag flow model

2.1 Momentum conservation

Same momentum balance equation used in previous analytical models was applied and, from Figure 2, it can be written as follow [3,4]:

AEC0016

Nomenclature

Symbols

□ = heat transfer area (m²)
□□□ = slag specific heat (J/kg·K)
□□ = slag specific heat (J/kg·K)
□ = diameter of reactor (m)
□□□□□ = gas-slag convection heat transfer coefficient (W/m²·K)
□□□□ = gas-slag radiation heat transfer coefficient (W/m²·K)
□ = slag thermal conductivity (W/m·K)
□□ = metal thermal conductivity (W/m·K)
□□□□□ = refractory wall thermal conductivity (W/m·K)
□̇□ = particle deposition rate (kg/s)
□̇□□ = gas flux (kg/m²·s)
□̇□□ = gas-slag heat transfer rate (W)
□̇□□□□ = heat transfer rate to solid slag (W)
□□ = metal temperature (K)
□□ = particle temperature (K)
□□ = surface temperature (K)
□□□ = internal wall temperature (K)
□□□ = external wall temperature (K)
□ = velocity (m/s)
z = distance from the liquid slag surface (m)

Greek letters

□ = angle of the wall (degree)
□□ = liquid slag thickness (m)
□□ = metal thickness (m)
□□ = solid slag thickness (m)
□□□□□ = refractory wall thickness (m)
□□ = gas viscosity (Pa·s)
□□ = slag viscosity (Pa·s)
□ = slag density (kg/m³)

$$\frac{□}{□□}\left(□□\frac{□□}{□□}\right) = -□□□□□□ \quad (3)$$

With boundary condition:

$$□ = 0\,; \quad □□\frac{□□}{□□} = 0$$
$$□ = □□\,; \quad □ = 0$$

Based on Seggiani's approach, viscosity can be approximate by following equation:

$$□(□) = □_0□□□\left(-\frac{□□}{□□}\right)$$

where

$$□ = -□□\left(\frac{□(□□)}{□_0}\right)$$

The solution of Eq. (3) gives:

$$□(□) = \frac{□□□□^2□□□□}{□_0□^2}\left[□^□(□-1) - □^{\frac{□□}{□□}}\left(\frac{□□}{□□}-1\right)\right] \quad (4)$$

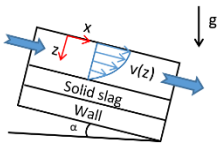

Figure 2. Momentum balance of finite control volume

2.2 Mass conservation

The mass balance equation at steady-state can be written as

$$□̇□□ = □̇□□□ + □̇□ \quad (5)$$

where □̇□□ is the leaving flow rate of slag from previous cell, □̇□□□ is the leaving flow rate of slag from current cell (see Figure 3.)

Integrate Eq. (4) through the liquid slag thickness, the leaving mass flow rate is obtained:

$$□̇□□□ = \int_0^{□□} □□□□(□)□□ \quad (6)$$

The solution of Eq. (6) is:

$$□̇□□□ = \frac{□^2□□□□□^3□□□□}{□_0□^3}\left[□^□(□^2 - 2□ + 2) - 2\right] \quad (7)$$

From equation (6), the molten slag thickness, □□, can be calculated.

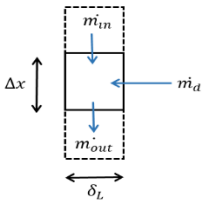

Figure 3. Mass balance of finite control volume

2.3 Energy conservation

Figure 4 shows the source of energy in and out of a finite control volume. From Fig. 4 the energy balance equation at steady-state can be written as:

$$□̇□□□ = □̇□□ - □̇□□□□ + □̇□□ + □̇□□□□ \quad (8)$$

where □̇□□ is heat flow rate from adjacent top cell.

Heat transfer from the gas phase to slag surface is usually described as:

$$□̇□□ = □(□□□□ + □□□□)(□□ - □□) \quad (9)$$

In our study, the coefficient of convective heat transfer between gas and molten slag were calculated an empirical correlation as follows [13]:

$$□□□□□ = \left[0.023\frac{(□□□□□)^{0.8}}{□^{0.2}}\right]\left(\frac{□□□^{0.4}□□^{0.6}}{□□^{0.4}}\right)\left(\frac{□□}{□□}\right)^{0.8}$$

where viscosity of gas mixture are estimated as [14]:

$$\square_{\square} = 1.98\times10^{-5}\times\left(\frac{\square_{\square}}{300}\right)^{2/3}$$

The coefficient of radiative heat transfer between gas and molten slag are calculated as follows [15]:

$$\square_{\square\square\square} = \square\square\left(\square_{\square}^{\ 2} + \square_{\square}^{\ 2}\right)\left(\square_{\square} + \square_{\square}\right)$$

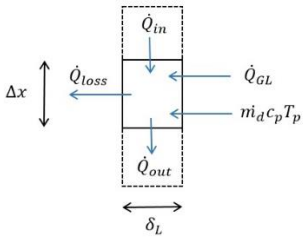

Figure 4. Energy balance of finite control volume

Employing the proposed cubic temperature profile across the molten slag layer, the exit heat transfer rate for current cell $\dot{\square}_{\square\square\square}$ can be obtained by integration equation (10) through the liquid slag thickness:

$$\dot{\square}_{\square\square\square} = \int_0^{\square_{\square}} \square\square\square\square_{\square}\square(\square)\square(\square)\square\square \qquad (10)$$

By substituting $T(z)$ [from equation (2)] and $v(z)$ [from equation (4)] in equation (10) $\dot{\square}_{\square\square\square}$ can be described.

As the axial heat conduction is neglected as listed in assumptions, the heat loss from the molten slag layer can represent with equation (11):

$$\dot{\square}_{\square\square\square\square} = -\square\square\left.\frac{\square\square}{\square\square}\right|_{\square_{\square}} = \square\square\left(\frac{1.5(\square_{\square}-\square_{\square\square})}{\square_{\square}} - \frac{\dot{\square}_{\square\square}}{2\square}\right) \qquad (11)$$

By substituting equation (9) - (11) into equation (8) the molten slag surface temperature (T_s) can be calculated using equation (12). T_s is the one and only key parameter that will have to return to gasifier model as shown in Figure 1. Here, it has to be noted that equation (12) is the main contribution of this study.

$$T_s = \frac{\dot{Q}_{in} + \dot{m}_d C_p T_p - T_{cv}\left\{C_3\left[\frac{3}{8}C_4 + 1.5C_5 - 0.5C_6 - e^{\square}(\square - 2) - 2\right] - \frac{1.5kA}{\delta_L}\right\} + (h_{conv} + h_{rad})T_g\left[\frac{3A}{2} + \frac{\delta_L C_3\left(\frac{C_4}{4} - C_5 + C_6\right)}{2k}\right]}{C_3\left(\frac{5}{8}C_4 - 1.5C_5 + 0.5C_6\right) + \frac{1.5kA}{\delta_L} + (h_{conv} + h_{rad})\left[\frac{3A}{2} + \frac{\delta_L C_3\left(\frac{C_4}{4} - C_5 + C_6\right)}{2k}\right]} \qquad (12)$$

where C_3-C_6 are derived as:

$$C_3 = \frac{\rho^2 g\pi D C_p \delta_L^{\ 3}\sin\alpha}{\mu_0 \square^3} \qquad (13)$$

$$C_4 = e^{\square}(\square^2 - \square) \qquad (14)$$

$$C_5 = e^{\square}\left[\square - 2 - \left(\frac{\square^2 - 3\square + 3}{\square}\right)\right] + \frac{2\square + 3}{\square} \qquad (15)$$

$$C_6 = e^{\square}\left[\square - 2 - \left(\frac{3\square^2 - 9\square + 9}{\square}\right) + \left(\frac{3\square^3 - 12\square^2 + 24\square - 24}{\square^2}\right) - \left(\frac{\square^4 - 5\square^3 + 15\square^2 - 30\square + 30}{\square^3}\right)\right] + \left(2 + \frac{9}{\square} + \frac{24}{\square^2} + \frac{30}{\square^3}\right) \qquad (16)$$

Finally, the solid slag thickness can be calculated by equation (17) deriving from Figure 5.

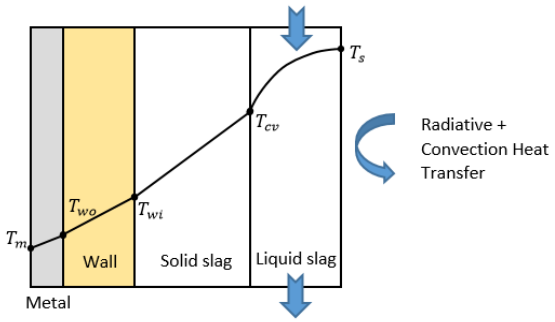

Figure 5. Cross section of slag along the reactor wall

$$\square_{\square} = \left[\frac{\square(\square_{\square\square} - \square_{\square})}{\dot{\square}_{\square\square\square\square}} - \frac{\square_{\square\square\square\square}}{\square_{\square\square\square\square}} - \frac{\square_{\square\square\square\square}}{\square_{\square\square\square\square}}\right]\square \qquad (17)$$

2.4 Slag and gas properties

Temperature and composition dependent slag properties (density, specific heat and thermal conductivity) were used in this study except for emissivity which was taken a constant value of 0.83 [16,17]. Viscosity of slag was calculated in the form of $\square = \square\square\ln(\square/\square)$ which A and B depend on chemical composition. In this study, A and B for each coals were calculated from data presented in an experimental study [18].

Specific heat of gas mixture were calculated an empirical correlation derived from JANAF data [19] and temperature dependent thermal conductivity of gas mixture were calculated using an equation proposed by Donskoi and McElwain [20].

2.5 Simulation conditions

The slag flow model was simulated using a 5MW pilot-scale gasifier which geometry and dimension are shown in Figure 6. Realistic operating condition were extracted from data reported in literature [21]. In the simulation, properties of two Australian coals (namely; CRC703 and CRC704) were used. Table 1 shown operating conditions defined for simulations. In Case 1, the slag flow model was simulated under typical gasification conditions where gas temperatures are higher than slag temperatures throughout the gasifier. In Case 2, all simulation conditions were set same as Case 1 except gas temperature at the bottommost section of gasifier, the entrance of tapping hole (highlighted grey in Figure 6) were defined as a fixed temperature of 1600K which was below critical viscosity temperature ($\square_{\square\square}$). In this study, ash deposition temperature ($\square_{\square}$) is assumed to a fixed temperature which is 50K lower than gas temperature (ie. $\square_{\square} = \square_{\square} - 50$) for both cases. During the simulation, the average temperature of the metal wall (T_m in Figure 5) is assumed to be kept a constant of 523K which was the same assumption made by Seggiani [3].

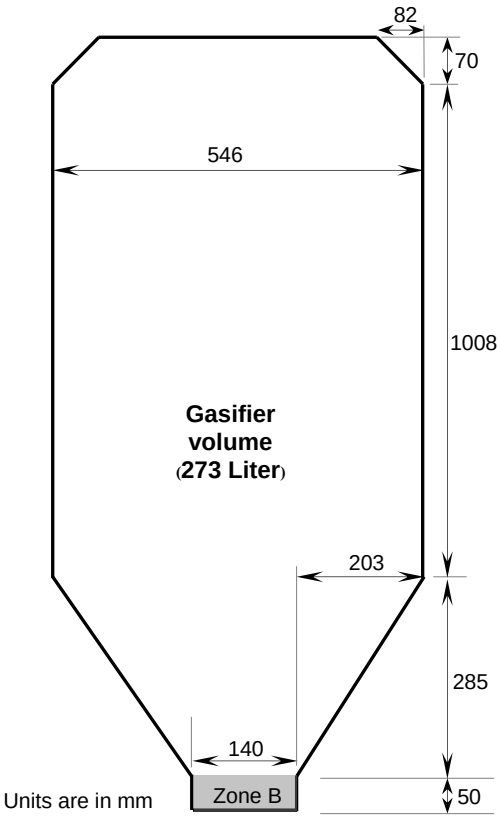

Figure 6. Geometry and dimensions of 5MW pilot-scale gasifier [21]

Table 1. Operating parameters set for simulations

Operating parameters	Case 1		Case 2	
	CRC 703	CRC 704	CRC 703	CRC 704
Gas temperature except Zone B (K)	1781	1834	1781	1834
Gas temperature at Zone B (K)	1781	1834	1600	1600
Gas flow rate, $\square_{\square}$ (kg/s)	1.25	1.25	1.25	1.25
Total particle deposition rate, $\square_{\square}$ (kg/s)	0.5	0.5	0.5	0.5
Particle Temperature, $\square_{\square}$ (K)	1731	1784	1731	1784

3. Simulation results and discussion

Operating conditions selected in previous section were used to conduct simulations using our analytical model, as well as using two other analytical models (namely, Seggiani's model [3] and Yong et al.'s model [4]) and the results were compared.

3.1 Case 1: Gas temperature > T_{cv}

The results obtained by simulating three different models under operating conditions listed in Case1 are shown in Figure 7 and Figure 8 representing for CRC703 and CRC704 respectively. Figures 7 and 8 present profiles of liquid slag thickness, solid slag thickness and liquid slag temperatures along the wall of gasifier. In this study, we assumed that slag deposits uniformly on the unit area of the gasifier wall. This assumption might not be representing what happens inside the gasifier where most of chars turn to slag usually concentrate near the hot combustion zone. However, this approach is simple and logical to access and evaluate the performances of different slag flow models without linking them with complex gasifier models.

All slag-flow models predict that both liquid and solid slags gradually accumulates and their depth getting thicker along the gasifier [see. Figure 7(a) & (b) and Figure 8(a) & (b)]. It was found that slag-surface temperatures changed significantly along the gasifier height even though gas temperature is set to a single value. It is mainly contributed by the thickness of slag changes along the height of gasifier. In general, more slag sticks to gasifier wall, smaller the heat-loss through reactor wall, as a result, liquid slag temperature is getting higher for the setting of a uniform gas temperature. From Figure 7(b) & (c) and Figure 8(b) & (c), it is apparent that increase of surface temperature is proportional to thickness of solid slag.

From Figure 7 and 8, it is also clear that performance of model developed in this study are much

more similar to that of Seggiani's model [3] rather than performances of the model developed by Yong et al. [4] for both coals under operating conditions of Case 1. According to finding of Ye and Ryu [12], performance of Seggiani's analytical model is similar to their numerical model's prediction under Case 1-like operation conditions. Therefore, it can be concluded that our analytical model's performance is comparable to prediction of complex numerical model developed by Ye and Ryu [12] for Case 1.

3.2 Case 2: Gas temperature < T_{cv}

As discussed in previous section, operating conditions set for Case 2 were same as those of Case 1 except for the section representing the entrance of the tapping hole (Zone B). For that particular section, gas temperature was set to be smaller than T_{cv} as presented in Table 1. Figure 9 and 10 shows the profiles of solid slag thickness, liquid slag temperatures and rate of heat loss along the height of gasifier wall for CRC703 and CRC704 respectively. The smaller graphs within the Figures were plotted by highlighting bottommost 0.15m of gasifier. All three models predicts same results as Figure 7 and 8 for the region above the tapping holes for Case 2 as same operating conditions defined as Case 1. Ye and Ryu [12] pointed out, performance of Seggiani's model was poor when gas temperature falls below critical viscosity temperature. This phenomena is reflecting Figure (9) and (10). As shown in Figure 9 (a) and 10 (a), slag thickness estimated by Seggiani's model was unrealistically large and consequently, it yields much smaller heat losses compared to the results estimated by Yong's model (see Figure 9 (c) and 10 (c)). Unlike, Seggiani's model, analytical model of Yong et al. [4] predicts well and agrees with performance of numerical model when gas temperature is lower than T_{cv} [12].

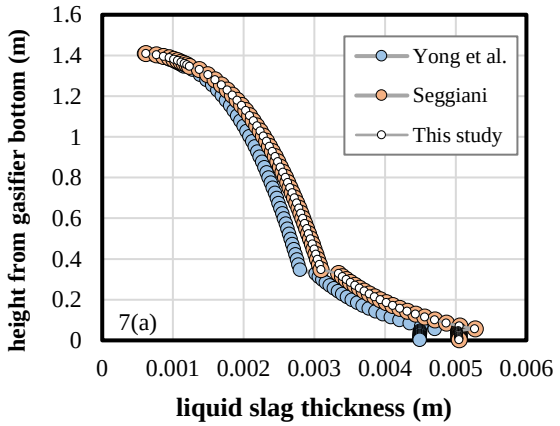

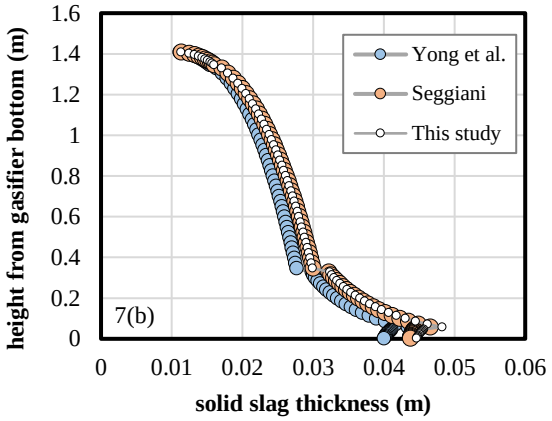

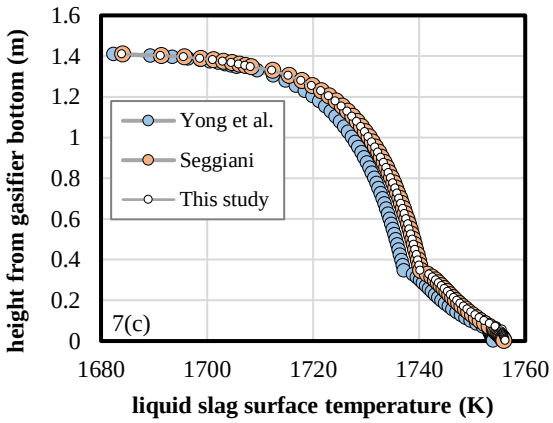

Figure 7. (a) Liquid slag thickness, (b) solid slag thickness (c) liquid slag surface temperature profiles along the height of gasifier wall simulated using methods proposed by three different models [for **CRC703** under ***Case 1***]

Figure (9) and (10) shows that our model's estimation follow the trend of results predicted by Yong et al. [4] within the bottommost region, even our model's predictions are much more similar to those calculated by Seggiani's model for the main gasifier region top of tapping hole. As our model combined assumptions made in both model, it eliminates the performance limitations of both models and it is found to be able to predict the slag behaviour more realistically regardless of local gas temperature being greater or smaller than T_{cv}.

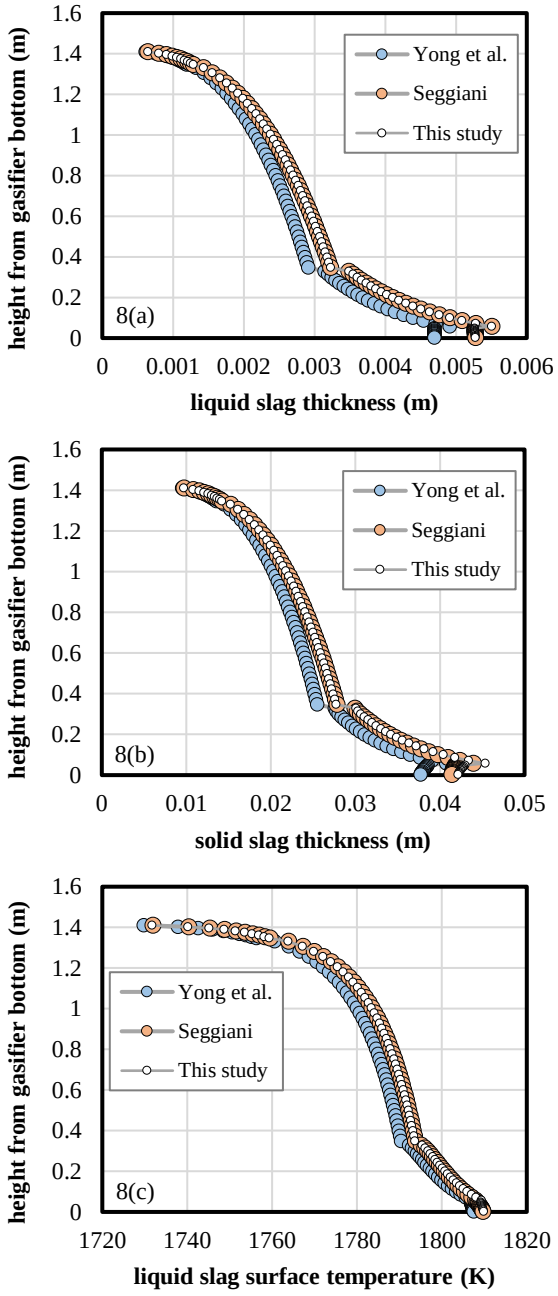

Figure 8. (a) Liquid slag thickness, (b) solid slag thickness (c) liquid slag surface temperature profiles along the height of gasifier wall simulated using methods proposed by three different models [for **CRC704** under ***Case 1***]

3.3 Effect of metal wall temperature on solid slag thickness

Figure (7) and (8) shows that solid slags formed along the wall are one-order of magnitude thicker than those of liquid slags. Thickness of solid slag is estimated using equation (17) which includes properties of refractory and metal walls. In this study, those properties were taken from Seggiani [3] and simulations were performed by assuming a uniform metal wall temperature of 523 K (T_m as labeled in Figure 5).

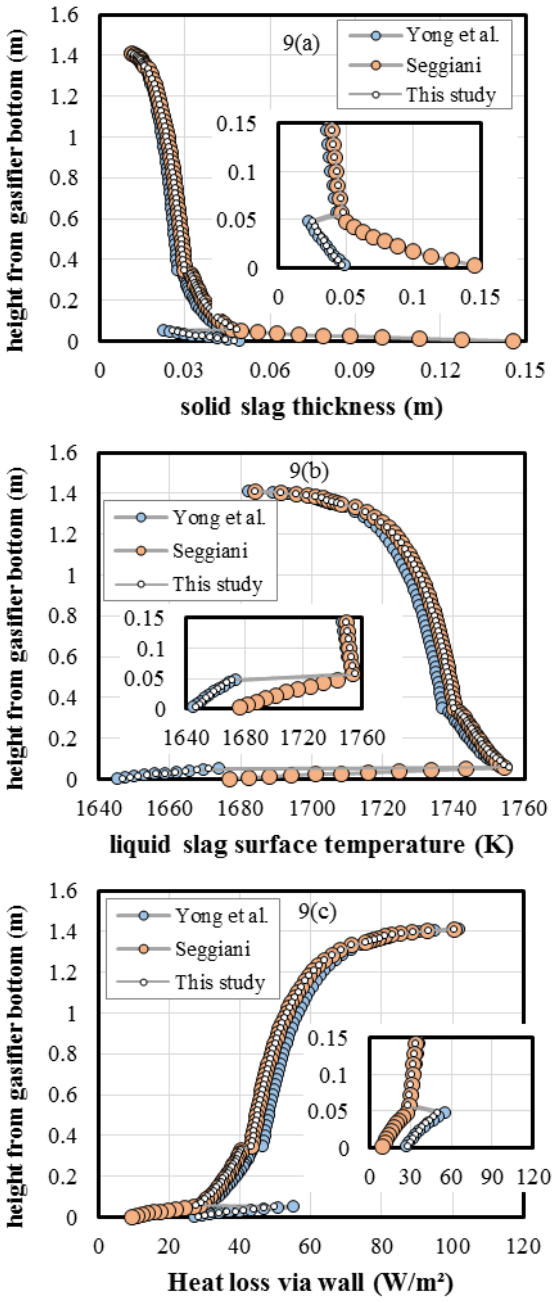

Figure 9. (a) Solid slag thickness, (b) liquid slag surface temperature (c) rate of heat loss profiles along the height of gasifier wall simulated using methods proposed by three different models [for **CRC703** under ***Case 2***]

To see the sensitivity of metal wall temperature on solid slag thickness, a set of simulation was performed by changing the T_m and the results were plotted in Figure 11. As expected, the relatively thinner solid slags were estimated when larger T_m were set. It is an apparent fact that the smaller amounts of solid slags were

AEC0016

required to yield the same amount of heat loss when minimum temperatures in a heat transfer process (T_m shown in Figure 5) were set as a higher value.

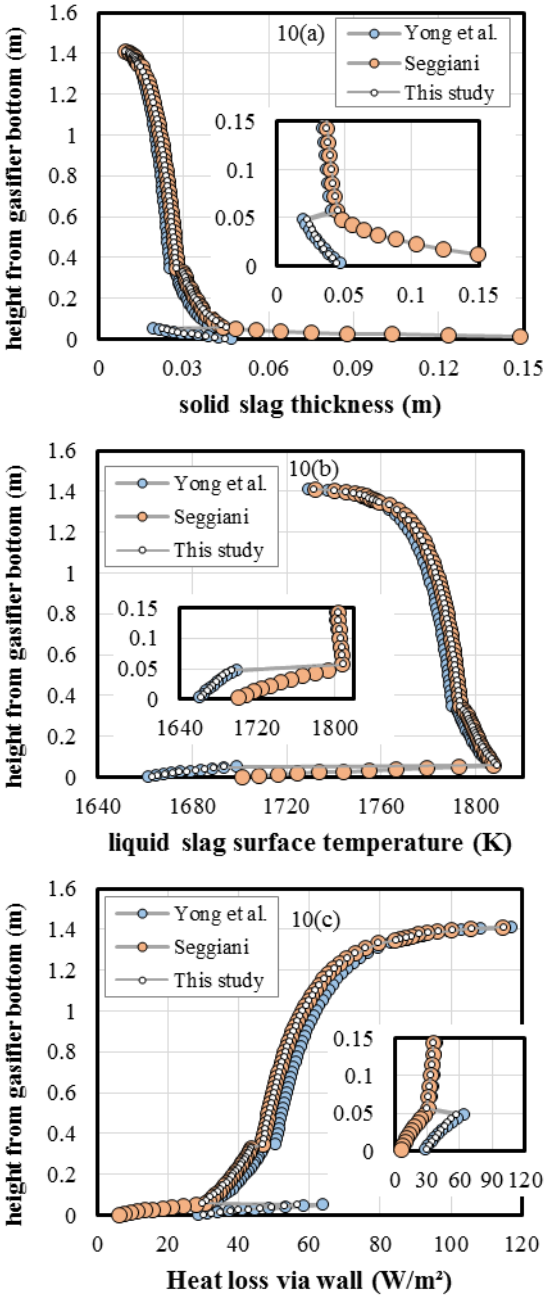

Figure 10. (a) Solid slag thickness, (b) liquid slag surface temperature (c) rate of heat loss profiles along the height of gasifier wall simulated using methods proposed by three different models [for **CRC704** under ***Case 2***]

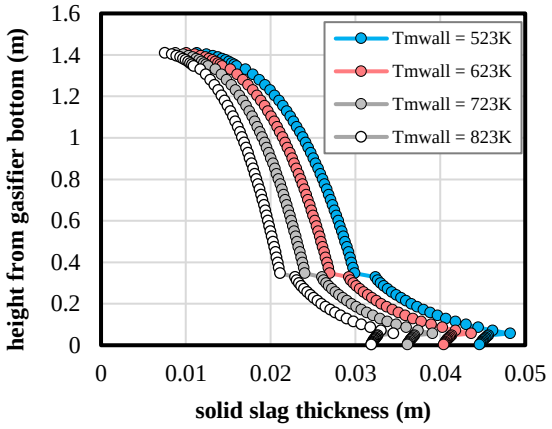

Figure 11. Effect of outside metal wall temperature on solid slag thickness profiles along the height of gasifier wall (Base line: Case1 with CRC703)

3.4 Effect of critical viscosity temperature (T_{cv}) on behaviour of slag flow

T_{cv} is one of the most important parameters which significantly affects the behaviour of slag flow. However, there are a number of different definitions of T_{cv} which include temperature at which solid phases begin to crystallize; temperature below which there is very rapid rise in viscosity; temperature at which slag flow changes from Newtonian to non-Newtonian fluid [22]. Hence it gives an uncertainty or variation of T_{cv} values for some compositions as each of the described above events can happened at different temperatures.

To investigate the effects of T_{cv} on slag flow behaviour, a set of simulation was performed for CRC703 under operating conditions of Case 1 but changing only the values of T_{cv}. Figure 12 shows the impacts of T_{cv} on profiles of solid slag thickness, liquid slag thickness, liquid slag surface temperature and rate of heat loss profiles along the height of gasifier wall. A larger T_{cv} means that slag solidifies at higher temperature as a result, the solid slag getting thicker for same operating gas temperature (See Figure 12 (a)). By setting the T_{cv} 40K higher than its base-line value, the resulting solid slag thickness were found to be 25 percent less.

AEC0016

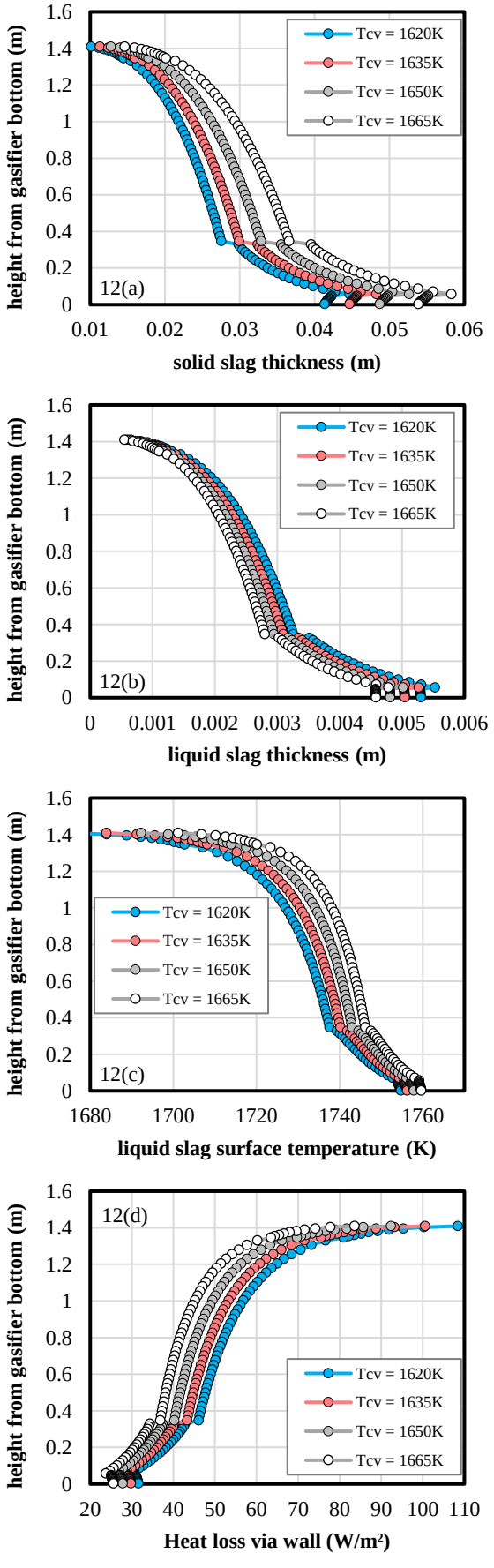

Figure 12. Effect of slag critical viscosity temperature on (a) solid slag thickness, (b) liquid slag thickness, (c) liquid slag surface temperature & (d) rate of heat loss profiles along the height of gasifier wall (Base line: Case1 with CRC703)

By setting the T_{cv} 40K higher than its base-line value, the resulting solid slag thickness were found to be 25 percent less. On a contrary to solid slag, a range of temperature, on which slag can exist in liquid form, was getting narrower and, thickness of liquid slag becomes smaller under higher T_{cv} as shown in Figure 12 (b). It is found that higher T_{cv} yield the hotter slag surface temperatures as shown in Figure 12(c). As thicker slags were formed for higher T_{cv}, rate of heat losses were found to be smaller when larger values of T_{cv} were set (See Figure 12 (d)).

4. Conclusion

An analytical slag flow model was developed and simulated to predict the slag behavior at steady-state for a 5MW pilot scale gasifier. This model was formulated by combining more realistic assumptions made in two analytical models previously developed. As a result, it was found that analytical models developed in this study can predict behaviour of slag flows more similar to the results calculated using complex numerical approach. More importantly, this model can predict slag behaviour under different operating gas temperatures whether they were higher or lower than critical viscosity temperatures. Our simulation results showed that the outer metal wall temperatures affect on the thickness of solid slag formed along the gasifier wall. As expected, changing the values of T_{cv} affects significantly on the behaviour of slag flow including liquid slag surface temperatures which is the only parameter returns as an input factor to gasifier model. Thus our future work is to integrate this analytical model to a gasifier model and, investigate how key parameters of slagging affect to the performance of entrained flow gasifiers.

5. References

[1] Ilyushechkin, A. Y. and Hla, S. S. (2013) Viscosity of high-iron slags from Australian coals, *Energy & Fuels*, vol. 27(7), July 2013, pp. 3736 – 3742.

[2] Chen, L., Yong, S. Z. and Ghoniem, A. (2013) Modeling the slag behavior in three dimensional CFD simulation of a vertically-oriented oxy-coal combustor, *Fuel Processing Technology*, vol. 112, August 2013, pp. 106 – 17.

[3] Seggiani, M. (1998) Modeling and simulation of time varying slag flow in a Prenflo entrained-flow gasifier, *Fuel*, vol. 77(14), November 1998, pp. 1611 – 1621.

[4] Yong, S.Z., Gazzino, M. and Ghoniem, A. (2012) Modeling the slag layer in solid fuel gasification and

combustion – Formulation and sensitivity analysis, *Fuel*, vol. 92(1), February 2012, pp. 162 – 170.

[5] Goldman, S. R. (1981) A technique for computer simulation of time varying slag flow in a coal gasification reactor, *AIChE Journal*, vol. 27(5), September, 1981, pp. 869 – 872.

[6] Fan, J. R., Zha, X. D., Sun, P. and Cen, K. F. (2001) Simulation of ash deposit in a pulverized coal-fired boiler, *Fuel*, Vol. 80(5), April 2001, pp. 645 – 654.

[7] Wang, X. H., Zhao, D. Q., He, L. B., Jiang, L. Q., HE, Q. and Chen, Y. (2007) Modeling of a coal-fired slagging combustor: Development of a slag submodel, *Combustion and Flame*, Vol. 149(3), May 2007, pp. 249 – 260.

[8] Ni, J., Zhou, Z., Yu, G., Liang, Q., and Wang, F. (2010) Molten slag flow and phase transformation behaviors in a slagging entrained-flow coal gasifier, *Industrial & Engineering Chemistry Research*, vol. 49(23), pp. 12302 – 12310.

[9] Yong, S. Z. and Ghoniem, A. (2012) Modeling the slag layer in solid fuel gasification and combustion – Two-way coupling with CFD, *Fuel*, Vol. 97, July 2012, Pages 457 – 466.

[10] Bi, D., Guan, Q., Xuan, W. and Zhang, J. (2015) Combined slag flow model for entrained flow gasification, Fuel, vol. 150(15), June 2015, Pages 565 – 572.

[11] Pednekar, P., Bhattacharyya, D., Kasule, J. S., Turton, R. and Rengaswamy, R. (2016) Dynamic model of a slagging entrained-flow gasifier including models of slag transport, deposition, and slag layer, *Industrial & Engineering Chemistry Research*, vol. 55, pp. 279 – 292.

[12] Ye, I. and Ryu, C. (2015) Numerical modeling of slag flow and heat transfer on the wall of an entrained coal gasifier. *Fuel*, vol. 150(15), June 2015, pp. 64 – 74.

[13] Babcock and Wilcox (1992). Steam: Its generation and use, The Babcock & Wilcox Company, Charlotte, North Carolina, USA.

[14] White, F. M. (1979). Fluid Mechanics, McGraw-Hill, New York, USA.

[15] Cengel, Y. A. and Ghajar, A. J. (2015). Heat and Mass Transfer: Fundamentals and Applications, 5th Edition, McGraw-Hill Education, New York, USA.

[16] Mills, K.C. and Rhine, J. M. (1989a). The measurement and estimation of the physical properties of slags formed during coal gasification: 1. Properties relevant to fluid flow, *Fuel*, vol. 68(2), February 1989, pp. 193 – 200.

[17] Mills, K.C. and Rhine, J. M. (1989b). The measurement and estimation of the physical properties of slags formed during coal gasification: 2. Properties relevant to heat transfer, *Fuel*, vol. 68(7), July 1989, pp. 904 – 910.

[18] Ilyushechkin, A. Y., Roberts, D. G. and Harris, D. J. (2014). Characteristics of solid by-products from entrained flow gasification of Australian coals, *Fuel Processing Technology*, Vol. 118, February 2014, pp. 98 – 109.

[19] JANAF (JANAF thermochemical tables) (1985). in: M. Chase, J. Davies, D. Downey, R. Frurip, Syverud McDonald (Eds.), J. Phys. Chem. Ref. Data American Chemical Society and the American Institute of Physics, New York (1985), pp. 535 – 1667.

[20] Donskoi, E. and McElwain, D. L. S. (2003). Estimation and modeling of parameters for direct reduction in iron ore/coal composites: Part 1. Physical Parameters, *Metallurgical and Materials Transactions B*, vol. 34(1), February 2003, pp. 93–102.

[21] Hla, S. S., Roberts, D. G. and Harris, D. J. (2015). A numerical model for understanding the behaviour of coals in an entrained-flow gasifier, *Fuel Processing Technology*, vol. 134, June 2015, pp. 424 – 440.

[22] Vargas, S., Frandsen, F. J., Dam-Johansen, K. (2001). Rheological properties of high-temperature melts of coal ashes and other silicates, *Progress in Energy and Combustion Science*, vol. 27(3), March 2001, pp. 237–429.